Dynamical dark sectors and neutrino masses and abundances

Weiqiang Yang,[1,*] Eleonora Di Valentino,[2,†] Olga Mena,[3,‡] and Supriya Pan[4,§]

[1]*Department of Physics, Liaoning Normal University, Dalian, 116029, People's Republic of China*
[2]*Jodrell Bank Center for Astrophysics, School of Physics and Astronomy, University of Manchester, Oxford Road, Manchester M13 9PL, United Kingdom*
[3]*Instituto de Fsica Corpuscular (CSIC-Universitat de Valencia), Parc Cientc UV, c/ Catedratico Jose Beltran 2, E-46980 Paterna, Spain*
[4]*Department of Mathematics, Presidency University, 86/1 College Street, Kolkata 700073, India*

(Received 6 April 2020; accepted 9 July 2020; published 22 July 2020)

We investigate generalized interacting dark matter–dark energy scenarios with a time-dependent coupling parameter, allowing also for freedom in the neutrino sector. The models are tested in the phantom and quintessence regimes, characterized by equations of state, $w_x < -1$ and $w_x > -1$, respectively. Our analyses show that for some of the scenarios, the existing tensions on the Hubble constant H_0 and on the clustering parameter S_8 can be significantly alleviated. The relief is either due to (a) a dark energy component which lies within the phantom region or (b) the presence of a dynamical coupling in quintessence scenarios. The inclusion of massive neutrinos into the interaction schemes does not affect either the constraints on the cosmological parameters or the bounds on the total number or relativistic degrees of freedom $N_{\rm eff}$, which are found to be extremely robust and, in general, strongly consistent with the canonical prediction $N_{\rm eff} = 3.045$. The most stringent bound on the total neutrino mass M_ν is $M_\nu < 0.116$ eV and it is obtained within a quintessence scenario in which the matter mass-energy density is only mildly affected by the presence of a dynamical dark sector coupling.

DOI: 10.1103/PhysRevD.102.023535

I. INTRODUCTION

Cosmological models where a nongravitational interaction between the dark fluids of the Universe, dark matter and dark energy, are still a very appealing and interesting solution to the so-called *why now?* problem. Early models were based on coupled quintessence scenarios [1–7], while more recent phenomenological approaches have adopted a number of possible parametrizations of the energy exchange rate; see, e.g., [8–54]. Following our pioneering previous work [55] we shall consider here a time-dependent coupling in nonminimal cosmologies. Given the fact that neutrinos can play a nonstandard role within nonminimal dark energy scenarios [56–66], we extend our previous analyses by inspecting the impact of neutrino properties within interacting cosmologies with a time-dependent coupling. We also generalize the work of Ref. [55] with the inclusion of a constant dark energy state parameter that may freely vary in a certain region. This picture also entails the case of a coupling parameter that remains constant in cosmic time. For our analyses we have assumed that our Universe is homogeneous and isotropic, that is, its geometry is well described by the Friedmann-Lemaître-Robertson-Walker (FLRW) line element. In order to perform robust statistical analyses, we shall make use of various cosmological datasets such as the Cosmic Microwave Background radiation, Baryon Acoustic Oscillation distance measurements, and, finally, a local measurement of the Hubble constant from the Hubble Space Telescope.

The manuscript has been organized as follows: In Sec. II we briefly introduce the gravitational equations for the two interacting dark fluids. Section III describes the observational data, methodology, and the priors imposed on the cosmological parameters. Section IV presents the current observational constraints on the interacting cosmic scenarios considered here. Section V contains our main conclusions.

II. INTERACTING DARK SECTORS: GRAVITATIONAL EQUATIONS

Observations suggest that at large scales, our Universe is homogeneous and isotropic and therefore well described by the FLRW line element

$$ds^2 = -dt^2 + a^2(t)\left[\frac{dr^2}{1-\kappa r^2} + r^2(d\theta^2 + \sin^2\theta d\phi^2)\right], \quad (1)$$

where $a(t)$ is the expansion scale factor of the Universe and (t, r, θ, ϕ) are the comoving coordinates. Having specified

[*]d11102004@163.com
[†]eleonora.divalentino@manchester.ac.uk
[‡]omena@ific.uv.es
[§]supriya.maths@presiuniv.ac.in

the metric of the underlying geometry of our Universe, we assume in the following that the gravitational sector of the Universe is described by general relativity, the matter sector is minimally coupled to gravity, and, finally, that there is a nongravitational interaction between the dark sectors of the Universe, namely, between the pressureless dark matter (DM) and the dark energy (DE) fluids:

$$\dot{\rho}_c + 3H\rho_c = -Q, \tag{2}$$

$$\dot{\rho}_x + 3H(1+w_x)\rho = Q, \tag{3}$$

where $H \equiv \dot{a}/a$ is the Hubble rate of the FLRW universe; ρ_c (p_c), ρ_x (p_x) are the energy density (pressure) for DM and DE, respectively (albeit the DM fluid, being pressureless here, has $p_c = 0$), $w_x = p_x/\rho_x$ denotes the barotropic DE equation of state parameter (assumed here to be constant) and, finally, Q determines the interaction rate between DM and DE. In general, when a specific form of the interaction rate is given, one can solve either analytically or numerically the background evolution for ρ_c and ρ_x. We shall explore here the (time-dependent) interacting dark energy (IDE) models of Ref. [55]:

$$\text{IDE1}: Q = 3\xi(a)H\rho_x, \tag{4}$$

$$\text{IDE2}: Q = 3\xi(a)H\frac{\rho_c\rho_x}{\rho_c+\rho_x}, \tag{5}$$

where $\xi(a)$ is a time-dependent dimensionless coupling parameter. Similar to our earlier work [55], we keep the parametrization of $\xi(a)$ as follows:

$$\xi(a) = \xi_0 + \xi_a(1-a), \tag{6}$$

where ξ_0 and ξ_a are real constants. Finally, based on the stability criteria of the perturbation evolution [12,13], we shall classify the models as

$$\text{IDE1p}: w_x < -1, \xi_0 < 0, \xi_a < 0, \tag{7}$$

$$\text{IDE1q}: w_x > -1, \xi_0 > 0, \xi_a > 0, \tag{8}$$

for the IDE1 case, and, equivalently,

$$\text{IDE2p}: w_x < -1, \xi_0 < 0, \xi_a < 0, \tag{9}$$

$$\text{IDE2q}: w_x > -1, \xi_0 > 0, \xi_a > 0, \tag{10}$$

for the IDE2 model, where p and q in IDEp and IDEq stand for *phantom* and *quintessence* regimes, respectively.

III. OBSERVATIONAL DATA AND METHODOLOGY

In the following we briefly describe the cosmological datasets used in this work.

(i) **Cosmic microwave background (CMB)**: our default dataset is the one containing the latest CMB temperature and polarization measurements in both the high and low multipole regions, i.e., Plik TT, TE, EE + lowl + lowE, from the final 2018 Planck legacy release [67–69].

(ii) **Baryon acoustic oscillations (BAO)**: we make use of several BAO measurements from different cosmological observations, as considered by the Planck Collaboration [67]: 6dFGS [70], SDSS-MGS [71], and BOSS DR12 [72] surveys.

(iii) **Hubble constant Gaussian prior (R19)**: we assume a Gaussian prior on the Hubble constant, in agreement with that obtained by the SH0ES Collaboration in 2019, i.e., $H_0 = 74.03 \pm 1.42$ km/s/Mpc at 68% CL [73].

For the analysis of the cosmological data, we adopt a fiducial model described by nine cosmological parameters. In particular, we vary the six parameters of the standard ΛCDM model, i.e., the baryon energy density $\Omega_b h^2$, the cold dark matter energy density $\Omega_c h^2$, the ratio between the sound horizon and the angular diameter distance at decoupling $100\theta_{MC}$, the reionization optical depth τ, the spectral index n_s, and the amplitude of the scalar primordial power spectrum A_s. In addition, we vary the three parameters of the dark sector physics considered here, i.e., the DE equation of state w_x and the strength of the coupling, parametrized by ξ_0 and ξ_a; see Eq. (6). The parameter space will therefore be described by

$$\mathcal{P} \equiv \{\Omega_b h^2, \Omega_c h^2, 100\theta_{MC}, \tau, n_s, \log[10^{10}A_s], \xi_0, \xi_a, w_x\}. \tag{11}$$

As aforementioned, the stability of the perturbation evolution restricts the IDE scenarios to two phantom cases ($w_x < -1$) [IDE1p, Eq. (7) and IDE2p, Eq. (9)] with $\xi_0 < 0$ and $\xi_a < 0$ and two quintessence regimes ($w_x > -1$) [IDE1q, Eq. (8) and IDE2q, Eq. (10)] with $\xi_0 > 0$ and $\xi_a > 0$. Table I lists the priors on all the parameters considered in this work.

We shall also consider an enlarged cosmological scenario with eleven parameters, allowing the sum of the neutrino masses M_ν and the number or relativistic degrees of freedom $N_{\rm eff}$ to freely vary (IDE + M_ν + $N_{\rm eff}$):

$$\mathcal{P} \equiv \{\Omega_b h^2, \Omega_c h^2, 100\theta_{MC}, \tau, n_s, \log[10^{10}A_s], \xi_0, \xi_a, w_x, M_\nu, N_{\rm eff}\}, \tag{12}$$

and also in this case we will have four cases, depending on the scenario of IDE considered and on the phantom or quintessence regime, i.e., IDE1p, IDE1q, IDE2p, and IDE2q, respectively.

To derive the constraints on the cosmological parameters we shall use a modified version with models IDE1 and

TABLE I. The table shows the flat priors imposed on various free parameters of the cosmological scenarios to be discussed in this work.

Parameter	Prior	Prior
$\Omega_b h^2$	[0.005, 0.1]	[0.005, 0.1]
$\Omega_c h^2$	[0.01, 0.99]	[0.01, 0.99]
τ	[0.01, 0.8]	[0.01, 0.8]
n_s	[0.5, 1.5]	[0.5, 1.5]
$\log[10^{10}A_s]$	[2.4, 4]	[2.4, 4]
$100\theta_{MC}$	[0.5, 10]	[0.5, 10]
w_x	$[-3, -1]$	$[-1, 0]$
ξ_0	$[-1, 0]$	[0, 1]
ξ_a	$[-1, 0]$	[0, 1]
M_ν	[0, 1]	[0, 1]
$N_{\rm eff}$	[0.05, 10]	[0.05, 10]

IDE2 implemented from the publicly available Markov chain Monte Carlo code CosmoMC [74,75] package. This version supports the new 2018 Planck likelihood [69] and uses a convergence diagnostic following the Gelman-Rubin criteria [76].

IV. RESULTS

A. IDE1

In the following we shall show the results obtained for the IDE1 scenario presented in Eq. (4), both in the phantom and in the quintessence regimes, and with and without varying the neutrino sector.

1. IDE1p

The results for the IDE1 model in the phantom regime, i.e., with $w_x < -1$, $\xi_0 < 0$ and $\xi_a < 0$, are reported in Table II and Fig. 1.

For an interacting dark energy with a phantomlike equation of state, the cold dark matter (CDM) energy density $\Omega_c h^2$ is larger than in the ΛCDM model, provided the energy transfer is from the DE to the DM sector [65,77]. Furthermore, due to the strong degeneracy between w_x and H_0, see Fig. 1, the Hubble constant is almost unconstrained for CMB only data. The well-known H_0 tension is strongly alleviated within this model. While ξ_0 has only a lower limit for all the combinations of data considered here, being therefore consistent with a vanishing interaction at present, we find ξ_a different from zero at 1 standard deviation for the CMB only ($\xi_a = -0.077^{+0.064}_{-0.032}$ at 68% CL) and for the CMB + R19 ($\xi_a = -0.077^{+0.059}_{-0.037}$ at 68% CL) cases. A very interesting feature of this model is the strong evidence for a phantomlike equation of state $w_x < -1$ for all the data combinations, with a statistical significance increasing from 1σ for the CMB only case ($w_x = -1.80^{+0.49}_{-0.39}$ at 68% CL) to about 2σ for CMB + BAO. Finally, the S_8 parameter moves towards lower values for the CMB only case, enough to bring it in agreement with the cosmic shear experiments DES [78,79], KiDS-450 [80–82], CFHTLenS [83–85], or the combination of KiDS+VIKING-450 and DES-Y1 [86], i.e., $S_8 = 0.789 \pm 0.037$ at 68% CL. However, when the BAO or the R19 priors are added to the CMB, the S_8 values are increased, restoring the tension at more than 3 standard deviations.

Finally, in Table X, we show the χ^2 values for this model, as well as other models considered in this work, for all the observational datasets employed here. In the same Table X, we have also shown the χ^2 values for the noninteracting scenario wCDM model as the reference model. From Table X we can see that the χ^2 values obtained for this scenario (i.e., IDE1p) are improved with

TABLE II. 95% CL constraints on the interacting scenario IDE1p using CMB from Planck 2018, BAO, and local measurements of H_0 from R19.

Parameters	Planck 2018	Planck 2018 + BAO	Planck 2018 + R19
$\Omega_c h^2$	$0.148^{+0.017}_{-0.019}$	$0.141^{+0.013}_{-0.014}$	$0.147^{+0.014}_{-0.018}$
$\Omega_b h^2$	$0.02246^{+0.00029}_{-0.00030}$	$0.02246^{+0.00030}_{-0.00030}$	$0.02244^{+0.00031}_{-0.00030}$
$100\theta_{MC}$	$1.0395^{+0.0012}_{-0.0011}$	$1.03989^{+0.00093}_{-0.00084}$	$1.0396^{+0.0010}_{-0.0010}$
τ	$0.053^{+0.016}_{-0.015}$	$0.055^{+0.016}_{-0.015}$	$0.053^{+0.015}_{-0.015}$
n_s	$0.9671^{+0.0088}_{-0.0091}$	$0.9678^{+0.0087}_{-0.0088}$	$0.9668^{+0.0087}_{-0.0090}$
$\ln(10^{10}A_s)$	$3.039^{+0.031}_{-0.030}$	$3.043^{+0.032}_{-0.031}$	$3.040^{+0.031}_{-0.031}$
w_x	> -2.53	$-1.21^{+0.20}_{-0.21}$	$-1.50^{+0.30}_{-0.31}$
ξ_0	> -0.061	> -0.084	> -0.071
ξ_a	> -0.16	> -0.091	> -0.15
Ω_{m0}	$0.27^{+0.13}_{-0.11}$	$0.341^{+0.039}_{-0.039}$	$0.310^{+0.036}_{-0.039}$
σ_8	$0.85^{+0.14}_{-0.14}$	$0.761^{+0.061}_{-0.058}$	$0.800^{+0.055}_{-0.049}$
H_0[km/s/Mpc]	> 63.9	$69.4^{+3.4}_{-3.3}$	$74.0^{+2.7}_{-2.7}$
S_8	$0.789^{+0.067}_{-0.068}$	$0.810^{+0.033}_{-0.035}$	$0.812^{+0.037}_{-0.042}$

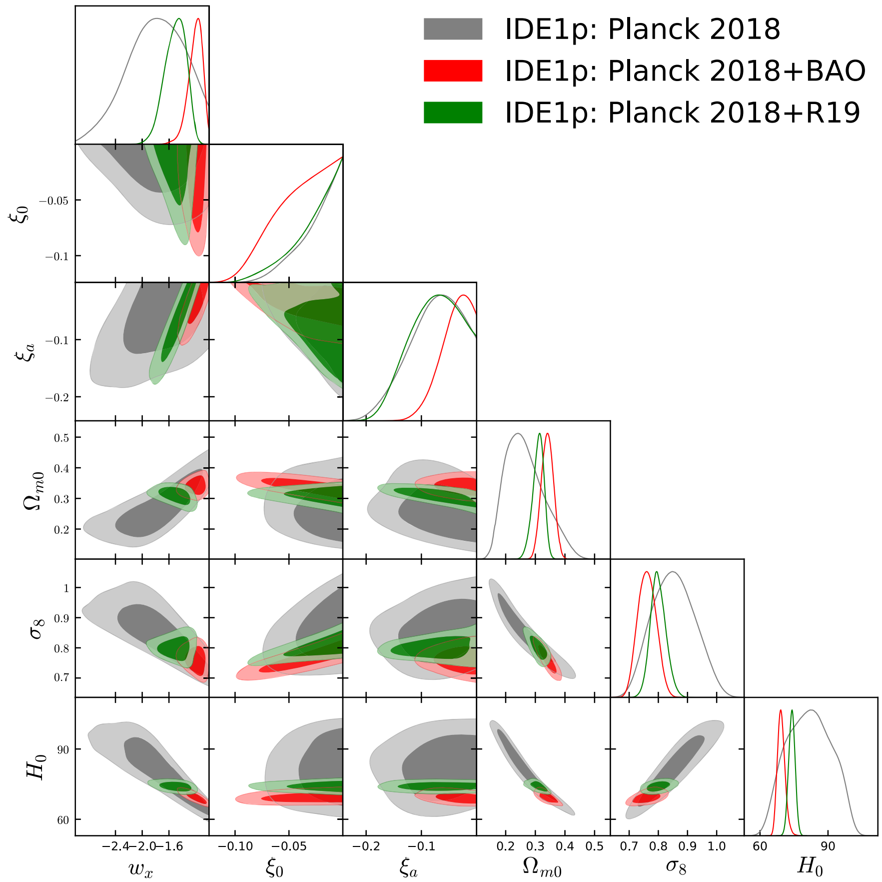

FIG. 1. One-dimensional marginalized posterior distributions and 68% and 95% CL two-dimensional contours for the interacting scenario IDE1p for the cosmological dataset combinations considered in this study.

respect to the wCDM model of about 2 (for Planck 2018 + BAO) and 4.5 (Planck 2018 + R19), even if in our case we have two more degrees of freedom compared to the wCDM model.

2. IDE1p + M_ν + $N_{\rm eff}$

The results for the IDE1 model in the phantom regime with the addition of the neutrino parameters, i.e., M_ν and $N_{\rm eff}$, are shown in Table III and Fig. 2.

The constraints from the previous section on the cosmological parameters and their correlations (IDE1p) are barely affected by allowing M_ν and $N_{\rm eff}$ to freely vary simultaneously. In particular, $\Omega_c h^2$ is larger than in the ΛCDM model and the Hubble constant tension with R19 is solved within 3σ even when BAO data are included. Also in this case ξ_0 has just a lower limit and is consistent with zero, while ξ_a is different from zero at 1 standard deviation for the CMB only ($\xi_a = -0.081^{+0.060}_{-0.037}$ at 68% CL) and CMB + R19 ($\xi_a = -0.087^{+0.055}_{-0.048}$ at 68% CL) cases, but consistent with zero when BAO data are included.

The indication for a phantom equation of state $w_x < -1$ is instead present for all the dataset combinations with a statistical significance always larger than 2 standard deviations, even for the CMB only case. The neutrino sector parameters M_ν and $N_{\rm eff}$ are mostly uncorrelated with the other cosmological parameters, with the exception of w_x that strongly anticorrelates with the total neutrino mass, M_ν. The existence of anticorrelation between w_x and M_ν is not new, in fact, in the usual noninteracting $w(z)$CDM cosmology, this has been already pointed out [59]; however, the interesting observation in this case that we find, even if the presence scenario allows an interaction in the dark sector, is that this anticorrelation does not get affected due to such interaction. The preference for $w_x < -1$ is therefore the reason for the much weaker upper limits on M_ν with respect to the same combinations of data within a ΛCDM model [59]. The most stringent limit we find on the sum of the neutrino masses is when adding BAO data to the CMB, i.e., $M_\nu < 0.162$ eV at 95% CL.

Regarding the constraints on the effective number of relativistic degrees of freedom $N_{\rm eff}$, these are completely unaffected by the inclusion of the interaction $\xi(a)$: in this scenario $N_{\rm eff}$ is always consistent with its expected value of 3.045 [87,88].

TABLE III. 95% CL constraints on the interacting scenario IDE1p $+ M_\nu + N_{\rm eff}$ using CMB from Planck 2018, BAO, and local measurements of H_0 from R19.

Parameters	Planck 2018	Planck 2018 + BAO	Planck 2018 + R19
$\Omega_c h^2$	$0.147^{+0.018}_{-0.019}$	$0.140^{+0.017}_{-0.017}$	$0.146^{+0.017}_{-0.019}$
$\Omega_b h^2$	$0.02235^{+0.00050}_{-0.00049}$	$0.02243^{+0.00046}_{-0.00044}$	$0.02234^{+0.00047}_{-0.00048}$
$100\theta_{MC}$	$1.0396^{+0.0013}_{-0.0012}$	$1.0400^{+0.0012}_{-0.0012}$	$1.0396^{+0.0013}_{-0.0012}$
τ	$0.053^{+0.015}_{-0.015}$	$0.055^{+0.016}_{-0.015}$	$0.053^{+00.016}_{-0.015}$
n_s	$0.963^{+0.018}_{-0.018}$	$0.966^{+0.018}_{-0.017}$	$0.963^{+0.018}_{-0.018}$
$\ln(10^{10}A_s)$	$3.036^{+0.036}_{-0.037}$	$3.041^{+0.037}_{-0.037}$	$3.036^{+0.037}_{-0.035}$
w_x	$-1.88^{+0.83}_{-0.81}$	$-1.21^{+0.20}_{-0.22}$	$-1.63^{+0.39}_{-0.44}$
ξ_0	> -0.067	> -0.083	> -0.066
ξ_a	> -0.16	> -0.090	> -0.17
Ω_{m0}	$0.27^{+0.14}_{-0.11}$	$0.341^{+0.041}_{-0.041}$	$0.311^{+0.039}_{-0.042}$
σ_8	$0.84^{+0.14}_{-0.13}$	$0.762^{+0.061}_{-0.060}$	$0.791^{+0.059}_{-0.054}$
H_0[km/s/Mpc]	81^{+18}_{-17}	$69.2^{+3.8}_{-3.6}$	$74.0^{+2.8}_{-2.9}$
M_ν[eV]	< 0.438	< 0.162	< 0.437
$N_{\rm eff}$	$2.96^{+0.40}_{-0.38}$	$3.01^{+0.40}_{-0.38}$	$2.96^{+0.41}_{-0.39}$
$\Omega_\nu h^2$	< 0.0047	< 0.0017	< 0.0046
S_8	$0.781^{+0.071}_{-0.076}$	$0.811^{+0.037}_{-0.037}$	$0.803^{+0.046}_{-0.048}$

In Table X we can see that the χ^2 values for this scenario (i.e., IDE1p $+ M_\nu + N_{\rm eff}$) are always below compared to the wCDM $+ M_\nu + N_{\rm eff}$ model, up to 4.2 for Planck 2018 + R19. We note that the model IDE1p $+ M_\nu + N_{\rm eff}$ has two more degrees of freedom compared to the wCDM $+ M_\nu + N_{\rm eff}$ model.

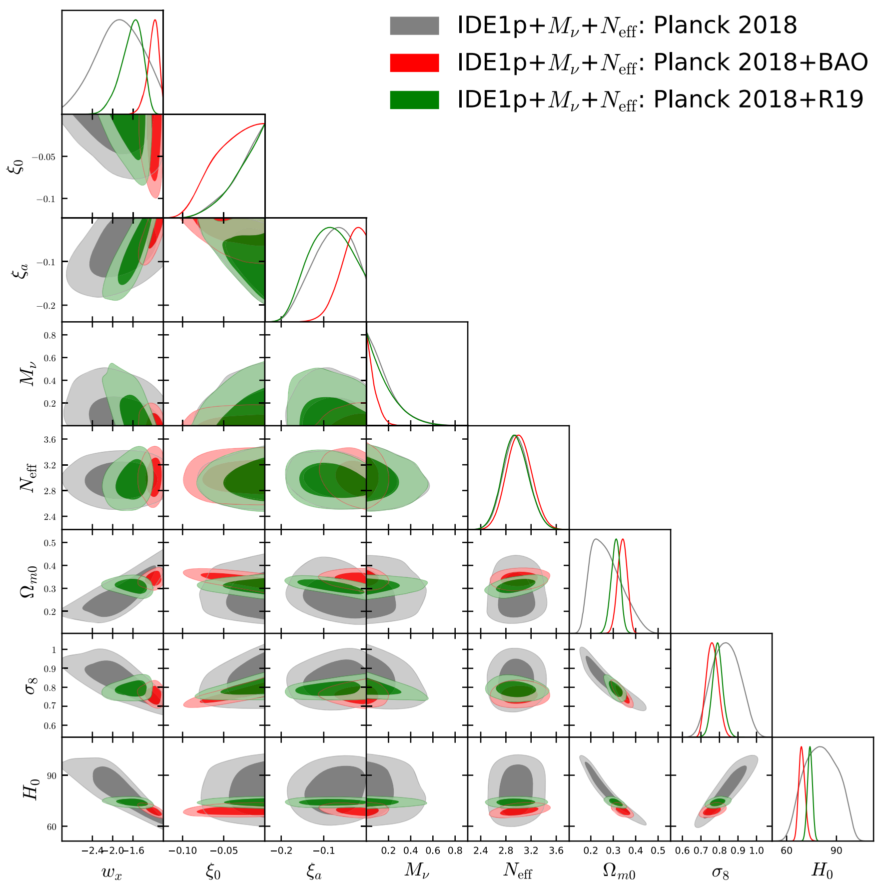

FIG. 2. One-dimensional marginalized posterior distributions and 68% and 95% CL two-dimensional contours for the interacting scenario IDE1p $+ M_\nu + N_{\rm eff}$ for the cosmological dataset combinations considered in this study.

TABLE IV. 95% CL constraints on the interacting scenario IDE1q using CMB from Planck 2018, BAO, and local measurements of H_0 from R19.

Parameters	Planck 2018	Planck 2018 + BAO	Planck 2018 + R19
$\Omega_c h^2$	< 0.109	$0.077^{+0.043}_{-0.058}$	< 0.075
$\Omega_b h^2$	$0.02232^{+0.00029}_{-0.00031}$	$0.02233^{+0.00029}_{-0.00029}$	$0.02234^{+0.00029}_{-0.00029}$
$100\theta_{MC}$	$1.0450^{+0.0048}_{-0.0042}$	$1.0436^{+0.0043}_{-0.0030}$	$1.0468^{+0.0034}_{-0.0035}$
τ	$0.054^{+0.016}_{-0.015}$	$0.055^{+0.016}_{-0.015}$	$0.054^{+0.016}_{-0.015}$
n_s	$0.9641^{+0.0088}_{-0.0089}$	$0.9647^{+0.0082}_{-0.0086}$	$0.9645^{+0.0086}_{-0.0086}$
$\ln(10^{10}A_s)$	$3.046^{+0.031}_{-0.031}$	$3.046^{+0.033}_{-0.032}$	$3.045^{+0.033}_{-0.031}$
w_x	< -0.77	< -0.77	< -0.89
ξ_0	< 0.25	< 0.22	$0.19^{+0.10}_{-0.12}$
ξ_a	< 0.046	< 0.043	< 0.054
Ω_{m0}	$0.17^{+0.16}_{-0.14}$	$0.22^{+0.10}_{-0.13}$	$0.106^{+0.086}_{-0.071}$
σ_8	$1.7^{+2.0}_{-1.2}$	$1.2^{+1.1}_{-0.6}$	$2.2^{+1.9}_{-1.4}$
H_0[km/s/Mpc]	$70.2^{+6.7}_{-7.1}$	$68.4^{+2.7}_{-2.5}$	$73.6^{+2.3}_{-2.5}$
S_8	$1.06^{+0.49}_{-0.31}$	$0.95^{+0.33}_{-0.19}$	$1.19^{+0.45}_{-0.38}$

3. IDE1q

The results for the IDE1 model in the quintessence regime, Eq. (8), are reported in Table IV and Fig. 3.

For an interacting dark energy with a quintessencelike equation of state, the CDM energy density $\Omega_c h^2$ is always smaller than in a ΛCDM model: indeed, only an upper limit for this cosmological parameter is found [65,77,89]. The most interesting feature of this IDE1q scenario is that, even if the well-known anticorrelation between w_x and H_0 is present, see Fig. 3, the positive correlation between ξ_0 and

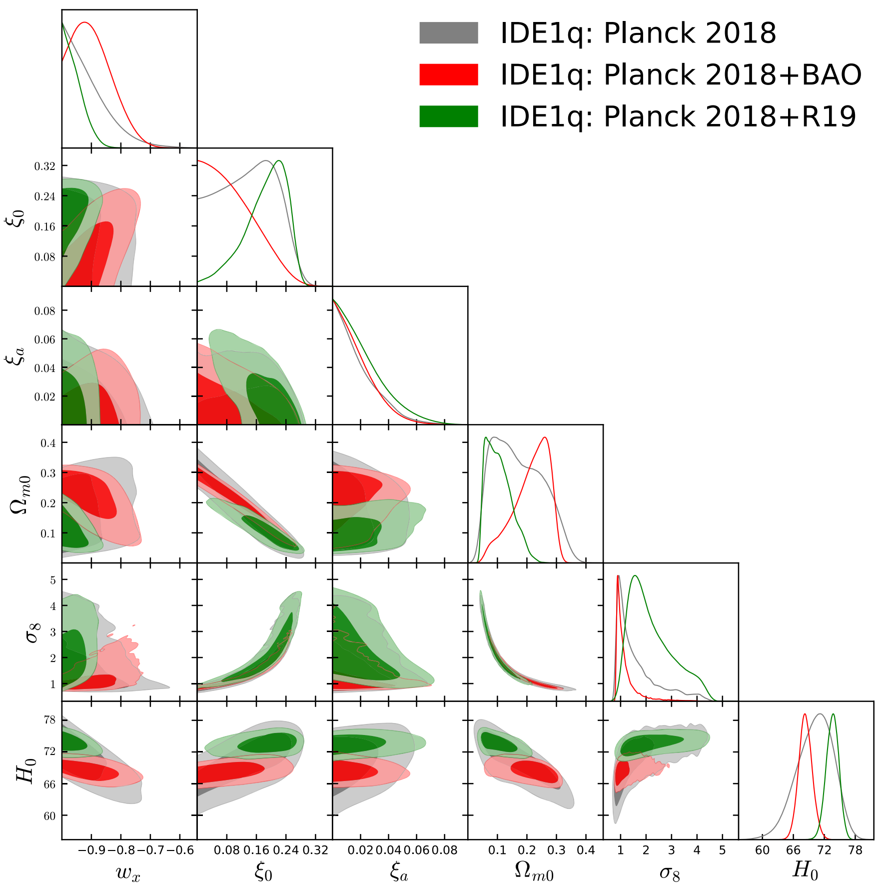

FIG. 3. One-dimensional marginalized posterior distributions and 68% and 95% CL two-dimensional contours for the interacting scenario IDE1q for the cosmological dataset combinations considered in this study.

TABLE V. 95% CL constraints on the interacting scenario IDE1q $+ M_\nu + N_{\rm eff}$ using CMB from Planck 2018, BAO, and local measurements of H_0 from R19.

Parameters	Planck 2018	Planck 2018 + BAO	Planck 2018 + R19
$\Omega_c h^2$	< 0.108	$0.075^{+0.043}_{-0.057}$	< 0.076
$\Omega_b h^2$	$0.02217^{+0.00046}_{-0.00046}$	$0.02223^{+0.00040}_{-0.00041}$	$0.02229^{+0.00041}_{-0.00041}$
$100\theta_{MC}$	$1.0450^{+0.0048}_{-0.0040}$	$1.0439^{+0.0043}_{-0.0031}$	$1.0470^{+0.0034}_{-0.0039}$
τ	$0.054^{+0.016}_{-0.015}$	$0.054^{+0.015}_{-0.015}$	$0.054^{+0.016}_{-0.015}$
n_s	$0.958^{+0.018}_{-0.017}$	$0.960^{+0.016}_{-0.016}$	$0.963^{+0.015}_{-0.015}$
$\ln(10^{10}A_s)$	$3.038^{+0.039}_{-0.037}$	$3.039^{+0.036}_{-0.036}$	$3.043^{+0.037}_{-0.035}$
w_x	< -0.105	< -0.781	< -0.881
ξ_0	< 0.26	< 0.23	$0.19^{+0.10}_{-0.12}$
ξ_a	< 0.052	< 0.050	< 0.060
Ω_{m0}	$0.18^{+0.15}_{-0.14}$	$0.21^{+0.10}_{-0.13}$	$0.104^{+0.089}_{-0.070}$
σ_8	$1.6^{+1.9}_{-1.0}$	$1.2^{+1.1}_{-0.6}$	$2.2^{+1.8}_{-1.4}$
H_0[km/s/Mpc]	$68.7^{+6.8}_{-7.4}$	$67.8^{+3.1}_{-2.8}$	$73.3^{+2.5}_{-2.5}$
M_ν[eV]	< 0.326	< 0.189	< 0.221
$N_{\rm eff}$	$2.89^{+0.39}_{-0.37}$	$2.92^{+0.37}_{-0.36}$	$2.99^{+0.35}_{-0.33}$
$\Omega_\nu h^2$	< 0.0034	< 0.0020	< 0.0024
S_8	$1.04^{+0.47}_{-0.28}$	$0.95^{+0.32}_{-0.19}$	$1.19^{+0.43}_{-0.38}$

H_0 shifts the Hubble constant towards higher values, solving the H_0 tension within 1σ for the CMB only case ($H_0 = 70.2^{+4.1}_{-3.1}$ km/s/Mpc at 68% CL).

Contrarily to the IDE1p case, in this IDE1q scenario the value of ξ_0, i.e., the interaction today, is found to be different from zero at low (high) significance for the CMB (CMB + R19) data. While for the CMB only and the CMB+R19 cases only an upper limit on w_x is found, an indication at 1σ for $w_x > -1$ appears for CMB + BAO ($w_x = -0.895^{+0.040}_{-0.093}$ at 68% CL). In this scenario, the S_8 parameter moves towards larger values; however, the error bars are very large, enabling an agreement with cosmic shear experiments.

Finally, in Table X we can see that the χ^2 for this scenario (i.e., IDE1q) is systematically higher than the wCDM model; therefore, it is disfavored by the fit of the data.

4. IDE1q $+M_\nu + N_{\rm eff}$

The results for the IDE1 model in the quintessence regime extended to include the neutrino parameters are shown in Table V and Fig. 4.

Similarly to the phantom case, both the constraints on the cosmological parameters and the correlations presented above are robust and are not affected by the introduction of the neutrino parameters M_ν and $N_{\rm eff}$. As in the previous section, ξ_0 is found to be different from zero at 1 standard deviation for the CMB only dataset ($\xi_0 = 0.137^{+0.087}_{-0.089}$ at 68% CL), at several standard deviations for CMB + R19, and it has just an upper limit for the CMB + BAO case. In this extended scenario ξ_a is always consistent with zero, as well as w_x is consistent with -1 at 95% CL for all the data combinations.

Also in this case the only important correlation between the neutrino sector and the remaining cosmological parameters is the one present between M_ν and w_x. However, in this quintessence regime, the CMB only upper limit on M_ν is stronger than the one found in the phantom regime (see Ref. [59]), and including the R19 prior this upper bound becomes even stronger ($M_\nu < 0.221$ eV at 95% CL). We note here that similar to the $w(z)$CDM case explored in [59] the anticorrelation between M_ν and w_x remains unaltered in the presence of the interaction between these dark sectors. This is an important point which clarifies that the anticorrelation between M_ν and w_x seems to be independent of the coupling in the dark sector. The most stringent limit in this case we find on the sum of the neutrino masses is when adding BAO data to the CMB, i.e., $M_\nu < 0.189$ eV at 95% CL.

Finally, in this extended scenario (as in the phantom one), the constraints on the effective number of relativistic degrees of freedom $N_{\rm eff}$ are completely consistent with its canonical value $N_{\rm eff} = 3.045$ for all the data combinations.

In Table X we can see that the χ^2 values for this scenario (i.e., IDE1q $+ M_\nu + N_{\rm eff}$) are always larger than the wCDM $+ M_\nu + N_{\rm eff}$ model. Therefore, this case is also disfavored by the data.

B. IDE2

In the following we shall show the bounds on the cosmological parameters obtained for the IDE2 scenario, see Eq. (5), both in the phantom and in the quintessence regimes, and with and without varying the neutrino sector.

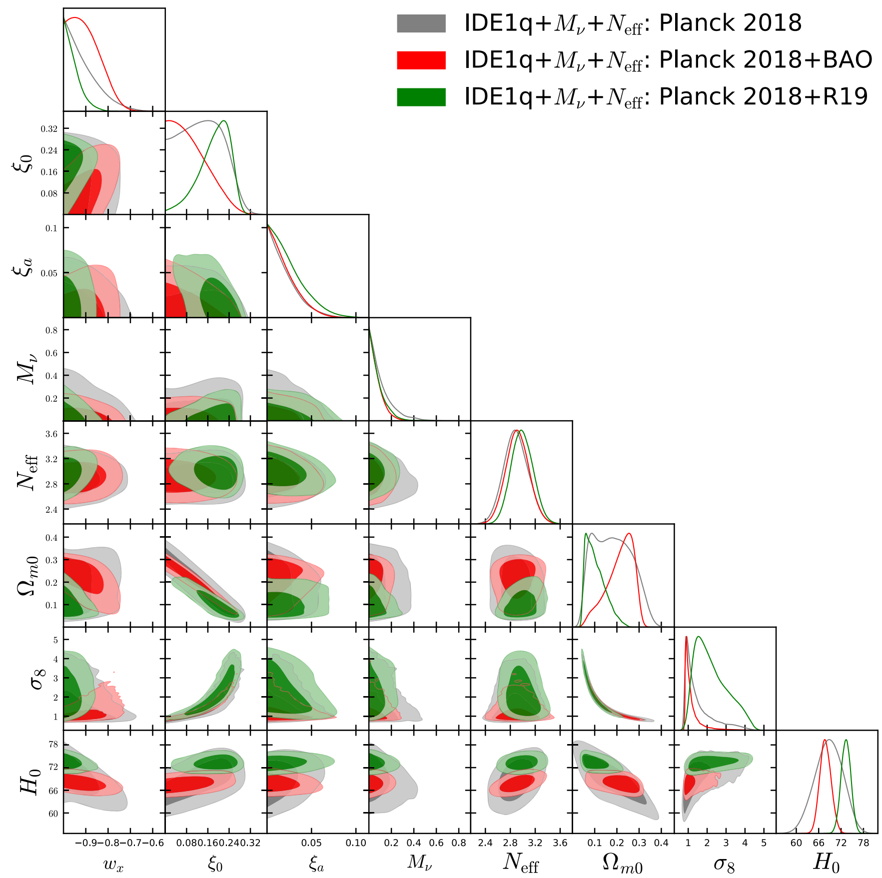

FIG. 4. One-dimensional marginalized posterior distributions and 68% and 95% CL two-dimensional contours for the interacting scenario IDE1q + M_ν + $N_{\rm eff}$ for the cosmological dataset combinations considered in this study.

1. IDE2p

The results for the IDE2 model in the phantom regime are reported in Table VI and Fig. 5.

In the IDE2 model, the interaction rate depends on both the cold dark matter density and the dark energy density. For this reason the flux of energy in the dark

TABLE VI. 95% CL constraints on the interacting scenario IDE2p using CMB from Planck 2018, BAO, and local measurements of H_0 from R19.

Parameters	Planck 2018	Planck 2018 + BAO	Planck 2018 + R19
$\Omega_c h^2$	$0.1203^{+0.0028}_{-0.0027}$	$0.1206^{+0.0024}_{-0.0023}$	$0.1208^{+0.0026}_{-0.0027}$
$\Omega_b h^2$	$0.02235^{+0.00029}_{-0.00030}$	$0.02231^{+0.00027}_{-0.00027}$	$0.02231^{+0.00029}_{-0.00029}$
$100\theta_{MC}$	$1.04088^{+0.00062}_{-0.00063}$	$1.04086^{+0.00059}_{-0.00060}$	$1.04083^{+0.00061}_{-0.00061}$
τ	$0.055^{+0.016}_{-0.015}$	$0.055^{+0.016}_{-0.015}$	$0.055^{+0.016}_{-0.016}$
n_s	$0.9639^{+0.0083}_{-0.0088}$	$0.9629^{+0.0080}_{-0.0079}$	$0.9627^{+0.0086}_{-0.0082}$
$\ln(10^{10}A_s)$	$3.046^{+0.032}_{-0.031}$	$3.048^{+0.032}_{-0.031}$	$3.047^{+0.034}_{-0.031}$
w_x	$-1.67^{+0.48}_{-0.37}$	> -1.173	$-1.25^{+0.10}_{-0.10}$
ξ_0	> -0.65	> -0.41	> -0.49
ξ_a	unconstrained	> -0.72	> -0.85
Ω_{m0}	$0.186^{+0.084}_{-0.055}$	$0.298^{+0.021}_{-0.022}$	$0.260^{+0.021}_{-0.019}$
σ_8	$0.93^{+0.12}_{-0.13}$	$0.797^{+0.048}_{-0.055}$	$0.834^{+0.055}_{-0.060}$
H_0[km/s/Mpc]	> 73	$69.4^{+2.6}_{-2.3}$	$74.4^{+2.8}_{-2.7}$
S_8	$0.725^{+0.081}_{-0.076}$	$0.795^{+0.045}_{-0.050}$	$0.776^{+0.052}_{-0.057}$

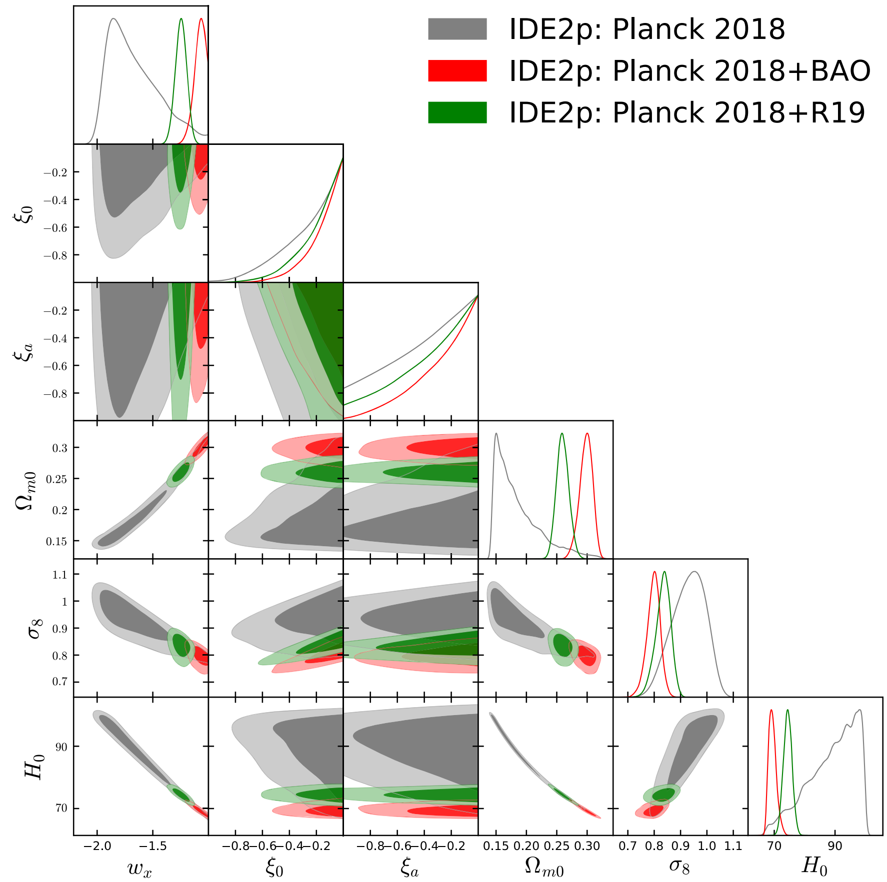

FIG. 5. One-dimensional marginalized posterior distributions and 68% and 95% CL two-dimensional contours for the interacting scenario IDE2p for the cosmological dataset combinations considered in this study.

sector, from DE to DM and vice versa, can change with time. In this scenario, the bound on the cold dark matter energy density $\Omega_c h^2$ is in perfect agreement with that obtained within a ΛCDM model, as we can notice from Table VI. The well-known negative correlation present between w_x and H_0 when w_x is in the phantom regime (see Fig. 5) shifts the Hubble constant towards much larger values. The H_0 tension is then reduced within 3 standard deviations for all the combinations of datasets considered in this work.

Both the interaction parameters ξ_0 and ξ_a have only a lower limit for all the dataset combinations at 68% CL and are consistent with zero, i.e., consistent with a model without interaction, as we notice from Table VI. Strong evidence for a phantom equation of state $w_x < -1$ is present at more than 2σ for the CMB only case and at many standard deviations for the CMB + R19 combination. However, this is not the case for CMB + BAO data. In this scenario IDE2p, the S_8 value shifts down enough to solve the tension with the cosmic shear experiments for all the data combinations considered here.

Finally, for this IDE2p scenario, we have that the χ^2 values are systematically higher than the wCDM model, as we can see in Table X, showing that this is disfavored by the fit of the data.

2. IDE2p + M_ν + $N_{\rm eff}$

The results for the IDE2 model within the phantom regime with the addition of the neutrino parameters, i.e., M_ν and $N_{\rm eff}$, are shown in Table VII and Fig. 6.

As in the IDE1 model, the results from the previous section are not modified significantly with the introduction of M_ν and $N_{\rm eff}$ as extra parameters. Indeed, in this scenario the bound on $\Omega_c h^2$ is really robust, shifted only 1 standard deviation towards lower values with respect to the case in which the neutrino parameters are fixed, but still in agreement with what is obtained in a ΛCDM model; see, e.g., Tables VI and VII. Also, here the Hubble constant is almost unconstrained when the CMB data only is considered, due to the negative correlation with w_x; see Fig. 6. For the very same reason, the H_0 tension is reduced within 2.5σ even after including BAO data in the analysis.

The neutrino sector parameters M_ν and $N_{\rm eff}$ do not show any strong correlation with the other cosmological

TABLE VII. 95% CL constraints on the interacting scenario IDE2p + M_ν + $N_{\rm eff}$ using CMB from Planck 2018, BAO, and local measurements of H_0 from R19.

Parameters	Planck 2018	Planck 2018 + BAO	Planck 2018 + R19
$\Omega_c h^2$	$0.1176^{+0.0059}_{-0.0058}$	$0.1179^{+0.0060}_{-0.0057}$	$0.1176^{+0.0060}_{-0.0057}$
$\Omega_b h^2$	$0.02215^{+0.00044}_{-0.00045}$	$0.02217^{+0.00040}_{-0.00040}$	$0.02210^{+0.00043}_{-0.00042}$
$100\theta_{MC}$	$1.04117^{+0.00089}_{-0.00087}$	$1.04118^{+0.00087}_{-0.00086}$	$1.04119^{+0.00087}_{-0.00088}$
τ	$0.054^{+0.016}_{-0.015}$	$0.055^{+0.016}_{-0.015}$	$0.053^{+0.015}_{-0.015}$
n_s	$0.956^{+0.016}_{-0.017}$	$0.956^{+0.015}_{-0.015}$	$0.954^{+0.016}_{-0.016}$
$\ln(10^{10}A_s)$	$3.036^{+0.038}_{-0.036}$	$3.039^{+0.036}_{-0.035}$	$3.036^{+0.036}_{-0.035}$
w_x	$-1.76^{+0.60}_{-0.45}$	> -1.22	$-1.33^{+0.18}_{-0.20}$
ξ_0	> -0.70	> -0.43	> -0.52
ξ_a	unconstrained	> -0.77	unconstrained
Ω_{m0}	$0.185^{+0.089}_{-0.057}$	$0.299^{+0.021}_{-0.024}$	$0.256^{+0.023}_{-0.022}$
σ_8	$0.92^{+0.13}_{-0.14}$	$0.791^{+0.050}_{-0.058}$	$0.825^{+0.062}_{-0.065}$
H_0[km/s/Mpc]	> 71	$68.7^{+3.3}_{-3.1}$	$74.2^{+2.7}_{-2.7}$
M_ν[eV]	< 0.365	< 0.181	< 0.339
$N_{\rm eff}$	$2.84^{+0.37}_{-0.36}$	$2.86^{+0.36}_{-0.35}$	$2.82^{+0.38}_{-0.35}$
$\Omega_\nu h^2$	< 0.0038	< 0.0019	< 0.0035
S_8	$0.714^{+0.083}_{-0.081}$	$0.789^{+0.048}_{-0.053}$	$0.762^{+0.056}_{-0.060}$

parameters, with the exception of w_x, which is anticorrelated with the total neutrino mass M_ν. As already pointed out, this anticorrelation between w_x and M_ν is independent of the coupling in the dark sector. The preference for $w_x < -1$ is the reason for the softening of the M_ν upper limit. The most stringent bound we find on

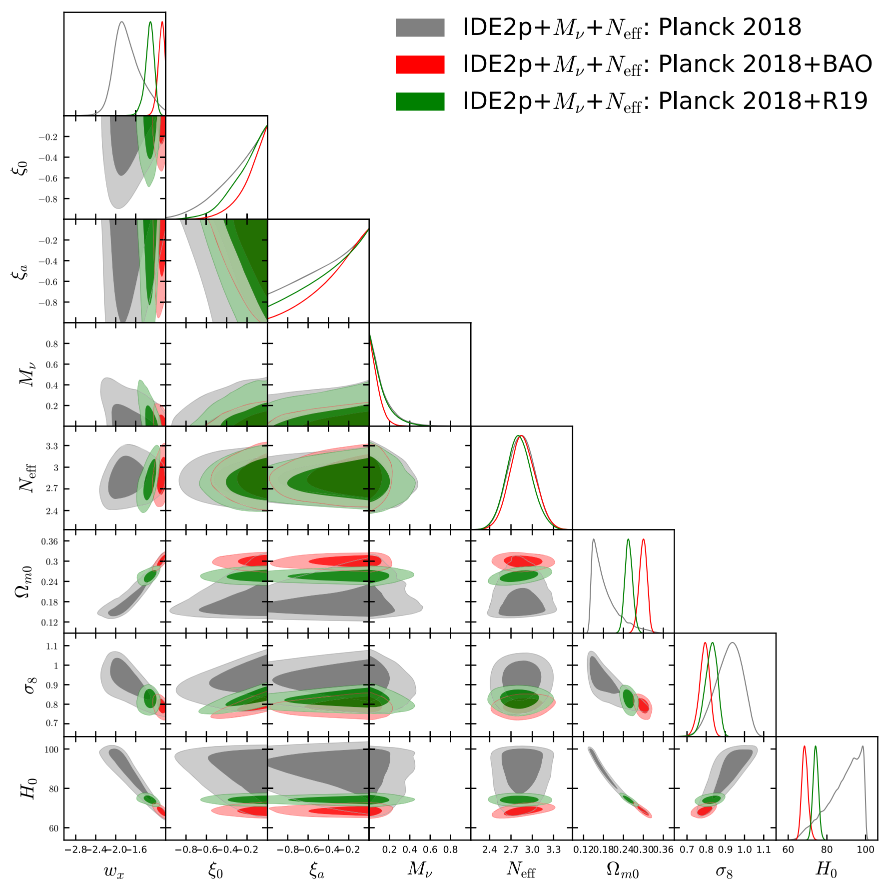

FIG. 6. One-dimensional marginalized posterior distributions and 68% and 95% CL two-dimensional contours for the interacting scenario IDE2p + M_ν + $N_{\rm eff}$ for the cosmological dataset combinations considered in this study.

TABLE VIII. 95% CL constraints on the interacting scenario IDE2q using CMB from Planck 2018, BAO, and local measurements of H_0 from R19.

Parameters	Planck 2018	Planck 2018 + BAO	Planck 2018 + R19
$\Omega_c h^2$	$0.1200^{+0.0026}_{-0.0027}$	$0.1188^{+0.0022}_{-0.0022}$	$0.1175^{+0.0025}_{-0.0025}$
$\Omega_b h^2$	$0.02238^{+0.00030}_{-0.00029}$	$0.02246^{+0.00028}_{-0.00028}$	$0.02258^{+0.00029}_{-0.00028}$
$100\theta_{MC}$	$1.04094^{+0.00060}_{-0.00062}$	$1.04108^{+0.00062}_{-0.00060}$	$1.04124^{+0.00060}_{-0.00058}$
τ	$0.053^{+0.016}_{-0.015}$	$0.054^{+0.015}_{-0.015}$	$0.057^{+0.016}_{-0.015}$
n_s	$0.9659^{+0.0089}_{-0.0085}$	$0.9689^{+0.0077}_{-0.0079}$	$0.9720^{+0.0082}_{-0.0082}$
$\ln(10^{10}A_s)$	$3.042^{+0.033}_{-0.032}$	$3.042^{+0.030}_{-0.032}$	$3.043^{+0.033}_{-0.033}$
w_x	< -0.79	< -0.925	< -0.975
ξ_0	< 0.159	< 0.195	< 0.224
ξ_a	< 0.36	< 0.37	< 0.44
Ω_{m0}	$0.337^{+0.049}_{-0.039}$	$0.316^{+0.017}_{-0.016}$	$0.302^{+0.015}_{-0.015}$
σ_8	$0.807^{+0.042}_{-0.054}$	$0.820^{+0.036}_{-0.033}$	$0.827^{+0.0326}_{-0.031}$
H_0[km/s/Mpc]	$65.2^{+3.3}_{-4.3}$	$67.1^{+1.5}_{-1.6}$	$68.3^{+1.2}_{-1.2}$
S_8	$0.855^{+0.038}_{-0.037}$	$0.841^{+0.036}_{-0.034}$	$0.830^{+0.040}_{-0.039}$

the sum of the neutrino masses is when adding BAO data to the CMB, i.e., $M_\nu < 0.181$ eV at 95% CL. The mean values of the effective number of relativistic degrees of freedom $N_{\rm eff}$ are lower than in a model without interaction $\xi(a)$, even if it is always highly consistent with its expected value $N_{\rm eff} = 3.045$.

In Table X we can see that the χ^2 value for Planck 2018 data for this scenario (i.e., IDE2p $+ M_\nu + N_{\rm eff}$) is larger

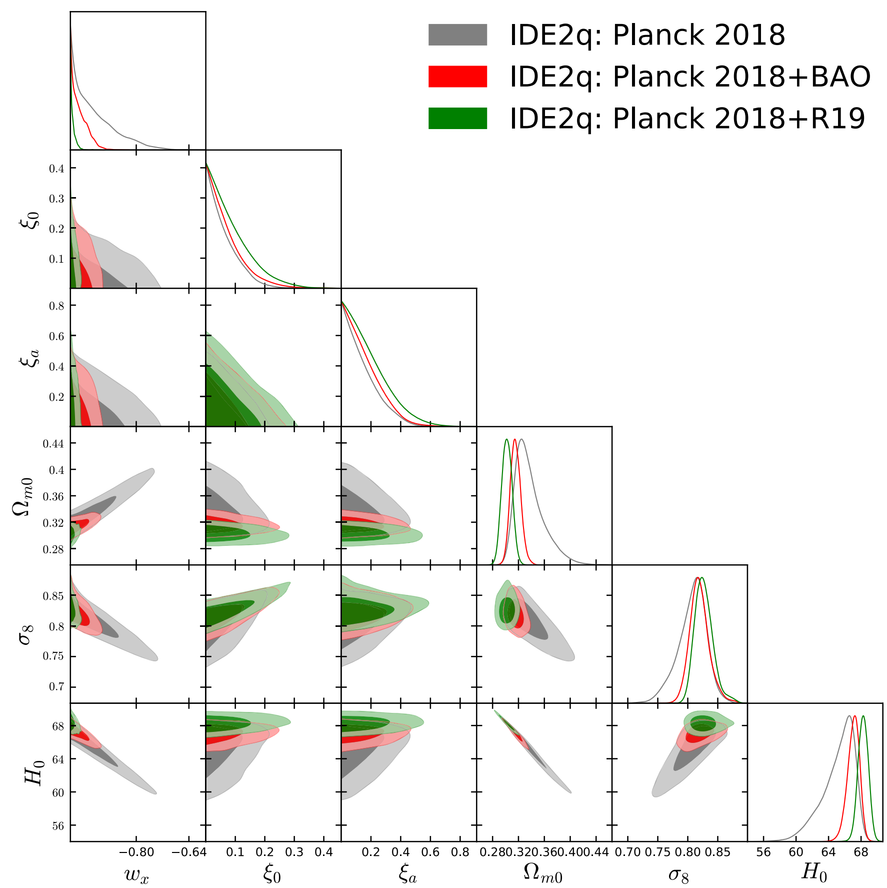

FIG. 7. One-dimensional marginalized posterior distributions and 68% and 95% CL two-dimensional contours for the interacting scenario IDE2q for the cosmological dataset combinations considered in this study.

TABLE IX. 95% CL constraints on the interacting scenario IDE2q + M_ν + $N_{\rm eff}$ using CMB from Planck 2018, BAO, and local measurements of H_0 from R19.

Parameters	Planck 2018	Planck 2018 + BAO	Planck 2018 + R19
$\Omega_c h^2$	$0.1187^{+0.0060}_{-0.0060}$	$0.1190^{+0.0060}_{-0.0061}$	$0.1237^{+0.0057}_{-0.0053}$
$\Omega_b h^2$	$0.02225^{+0.00046}_{-0.00046}$	$0.02247^{+0.00038}_{-0.00039}$	$0.02284^{+0.00034}_{-0.00034}$
$100\theta_{MC}$	$1.04105^{+0.00091}_{-0.00088}$	$1.04107^{+0.00089}_{-0.00084}$	$1.04057^{+0.00076}_{-0.00079}$
τ	$0.053^{+0.016}_{-0.015}$	$0.055^{+0.016}_{-0.015}$	$0.058^{+0.016}_{-0.016}$
n_s	$0.961^{+0.018}_{-0.018}$	$0.969^{+0.015}_{-0.015}$	$0.985^{+0.013}_{-0.013}$
$\ln(10^{10}A_s)$	$3.037^{+0.038}_{-0.036}$	$3.042^{+0.037}_{-0.036}$	$3.060^{+0.036}_{-0.034}$
w_x	< -0.77	< -0.915	< -0.965
ξ_0	< 0.17	< 0.17	< 0.23
ξ_a	< 0.39	< 0.39	< 0.48
Ω_{m0}	$0.353^{+0.068}_{-0.056}$	$0.315^{+0.018}_{-0.016}$	$0.294^{+0.018}_{-0.016}$
σ_8	$0.788^{+0.066}_{-0.075}$	$0.822^{+0.037}_{-0.036}$	$0.852^{+0.040}_{-0.038}$
H_0[km/s/Mpc]	$63.7^{+5.3}_{-5.8}$	$67.2^{+2.4}_{-2.5}$	$70.7^{+2.2}_{-2.1}$
M_ν[eV]	< 0.41	< 0.137	< 0.116
$N_{\rm eff}$	$2.94^{+0.39}_{-0.38}$	$3.06^{+0.36}_{-0.38}$	$3.43^{+0.15+0.32}_{-0.29}$
$\Omega_\nu h^2$	< 0.0043	< 0.00150	< 0.00129
S_8	$0.853^{+0.040}_{-0.038}$	$0.842^{+0.035}_{-0.033}$	$0.844^{+0.044}_{-0.037}$

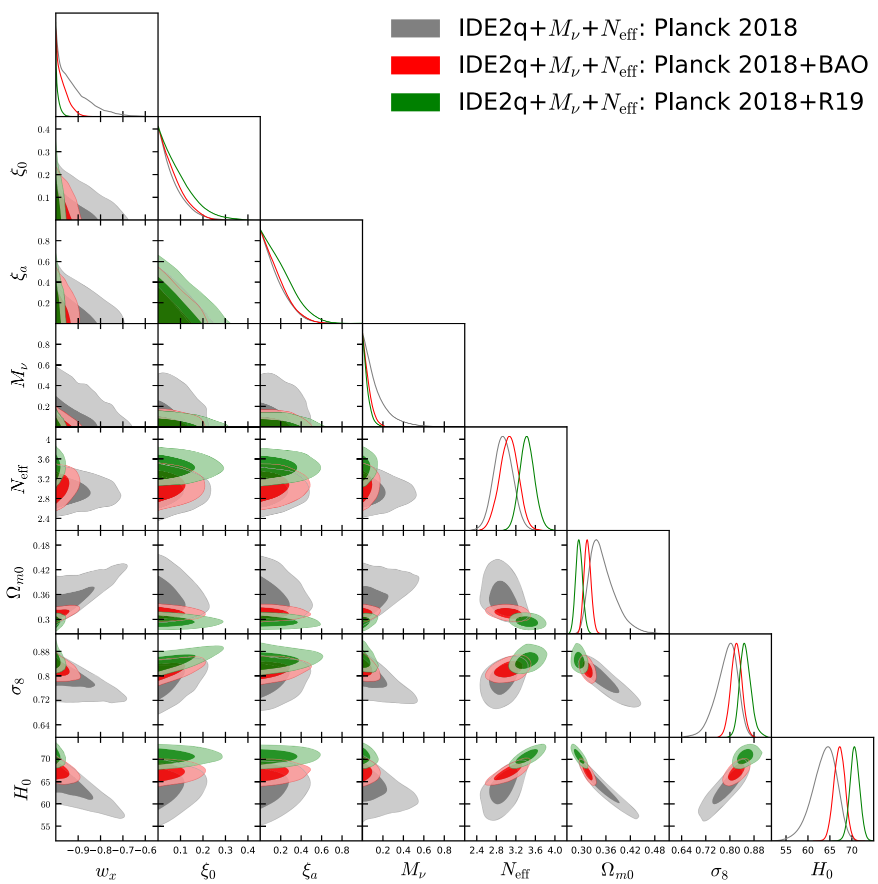

FIG. 8. One-dimensional marginalized posterior distributions and 68% and 95% CL two-dimensional contours for the interacting scenario IDE2q + M_ν + $N_{\rm eff}$ for the cosmological dataset combinations considered in this study.

TABLE X. Best fit χ^2 for the cases analyzed here and the comparison with wCDM and $w\mathrm{CDM} + M_\nu + N_{\mathrm{eff}}$ models.

Parameters	Planck 2018	Planck 2018 + BAO	Planck 2018 + R19
wCDM	2767.124	2777.664	2771.262
IDE1p	2767.166	2775.306	2766.776
IDE1q	2775.446	2780.372	2774.392
IDE2p	2769.308	2781.104	2773.456
IDE2q	2773.834	2779.528	2790.99
$w\mathrm{CDM} + M_\nu + N_{\mathrm{eff}}$	2768.422	2779.370	2771.166
$\mathrm{IDE1p} + M_\nu + N_{\mathrm{eff}}$	2766.376	2776.278	2766.948
$\mathrm{IDE1q} + M_\nu + N_{\mathrm{eff}}$	2773.570	2779.448	2774.210
$\mathrm{IDE2p} + M_\nu + N_{\mathrm{eff}}$	2769.558	2777.012	2770.830
$\mathrm{IDE2q} + M_\nu + N_{\mathrm{eff}}$	2775.076	2777.986	2782.564

than the corresponding χ^2 value obtained for the $w\mathrm{CDM} + M_\nu + N_{\mathrm{eff}}$ model, but concerning the other two datasets, the χ^2 values for $\mathrm{IDE2p} + M_\nu + N_{\mathrm{eff}}$ are lower than the $w\mathrm{CDM} + M_\nu + N_{\mathrm{eff}}$ model. However, these lower values are consistent with the introduction of two more degrees, so they do not correspond to an actual improvement of the fit. Therefore, these cases are almost equivalent.

3. *IDE2q*

The results for the IDE2 model in the quintessence regime, Eq. (10), are presented in Table VIII and Fig. 7.

In the IDE2q scenario, the well-known anticorrelation present between w_x and H_0 shifts the Hubble constant towards lower values, see Fig. 7, exacerbating the H_0 tension at more than 4σ with respect to previous models.

Both the interaction parameters ξ_0 and ξ_a are constrained by an upper limit for all the dataset combinations and are uncorrelated with the other cosmological parameters, as can be noticed from Fig. 7. Only an upper limit is present also for the equation of state in the quintessence regime $w_x > -1$, and the S_8 tension with the cosmic shear experiments is restored.

Finally, even this IDE2q scenario is disfavored by the fit of the data as showed in Table X.

4. $\mathrm{IDE2q} + M_\nu + N_{\mathrm{eff}}$

The results for the IDE2 model in the quintessence regime with M_ν plus N_{eff} as additional parameters are shown in Table IX and Fig. 8. However, for this model IDE2q, the neutrino parameters M_ν and N_{eff} are correlated with other cosmological parameters. In particular, we notice an important correlation with the Hubble constant H_0. This degeneracy is responsible, when the R19 prior is included in the data, i.e., for the combination CMB + R19, for the shift of N_{eff} towards higher values. The value $N_{\mathrm{eff}} = 3.43^{+0.15}_{-0.16}$ at 68% CL deviates from the canonical expectation more than 2 standard deviations. In this IDE2q scenario we obtain our strongest limit on the M_ν, $M_\nu < 0.116$ eV at 95% CL, as expected in quintessential noninteracting scenarios [59] where an antifcorrelation between w_x and M_ν exists similar to this coupled case.

In Table X we can see that the χ^2 values for $\mathrm{IDE2q} + M_\nu + N_{\mathrm{eff}}$ are larger than the χ^2 values obtained in the $w\mathrm{CDM} + M_\nu + N_{\mathrm{eff}}$ model for Planck 2018 alone and Planck 2018 + R19, but lower for Planck 2018 + BAO. However, this improvement quantified through $\Delta\chi^2 \sim 2$ is consistent with the fact that in the interacting scenario we have two extra degrees of freedom, so it does not correspond to an actual improvement of the fit.

V. SUMMARY AND CONCLUSIONS

In this manuscript we further investigate the presence of an exchange rate Q between DM and DE allowing for a time-dependent coupling [55]. We add new ingredients in the models, such as (i) freely varying neutrino parameters and (ii) a DE with a constant, freely varying equation of state, rather than vacuum dark energy. We restrict ourselves to the natural form of the coupling parameter $\xi(a) = \xi_0 + (1-a)\xi_a$ and consider two interacting models, namely, IDE1 ($Q = 3H[\xi_0 + \xi_a(1-a)]\rho_x$) and IDE2 ($Q = 3H[\xi_0 + \xi_a(1-a)]\frac{\rho_c\rho_x}{\rho_c+\rho_x}$). In order to avoid instabilities in the perturbation evolution, we consider the regions (A) $w_x < -1$, $\xi_0 < 0$, $\xi_a < 0$, and (B) $w_x > -1$, $\xi_0 > 0$, $\xi_a > 0$, and investigate the interacting scenarios with and without the presence of neutrinos. The scenario with phantom DE equation of state ($w_x < -1$) is labeled as IDEp and the scenario where DE has a quintessencelike equation of state ($w_x > -1$) is labeled as IDEq. Let us summarize the main observational results that we find for all these scenarios:

(i) IDE1: We have explored this interaction model for both regimes, namely, $w_x < -$ and $w_x > -1$ with and without the presence of neutrinos. We have therefore investigated four different scenarios: IDE1p, $\mathrm{IDE1p} + M_\nu + N_{\mathrm{eff}}$, IDE1q, and $\mathrm{IDE1q} + M_\nu + N_{\mathrm{eff}}$.

We find that for both IDE1p and IDE1p + $M_\nu + N_{\rm eff}$, $\Omega_c h^2$ is larger than within the ΛCDM cosmology and w_x prefers a phantom nature with high significance. The parameter ξ_0 determining the current value of the DM–DE interaction is consistent with a null value, while ξ_a prefers a value different from zero (albeit only mildly). We also notice that within these two phantom frameworks, the tension on H_0 is alleviated satisfactorily for all the data combinations considered here (CMB, CMB + BAO, and CMB + R19). Concerning the S_8 parameter, its tension is significantly reduced only for the case of CMB data alone. The inclusion of M_ν and $N_{\rm eff}$ to IDE1p does not change the constraints on other parameters. The most stringent bound on M_ν is obtained for the CMB + BAO case and is $M_\nu < 0.162$ eV at 95% CL.

As regards the remaining two scenarios IDE1q and IDE1q + $M_\nu + N_{\rm eff}$, similarly to the phantom case, the inclusion of the neutrinos does not affect the constraints on the remaining cosmological parameters. The tightest bound on M_ν appears for the CMB + BAO case ($M_\nu < 0.189$ eV at 95% CL) which is slightly larger than the one obtained within the ΛCDM framework for the same data combination. Contrarily to the previous two cases, the value of $\Omega_c h^2$ is much smaller. The parameter ξ_0 is found to be nonzero for all the cases. However, ξ_a is consistent with zero for all the datasets exploited in this work. The H_0 tension is solved for the CMB case ($H_0 = 70.2^{+4.1}_{-3.1}$ km/s/Mpc) and due to the very large error bars on the S_8 parameter, the S_8 tension is mildly alleviated.

(ii) IDE2: Using the very same observational data then for IDE1, we have investigated four scenarios, namely, IDE2p, IDE2p + $M_\nu + N_{\rm eff}$, IDE2q, and IDE2q + $M_\nu + N_{\rm eff}$.

The scenario IDE2p is very interesting because both the H_0 and S_8 tensions are alleviated for all the data combinations used in this analysis. The dark energy equation of state shows a strong preference for a phantom nature. When neutrinos are considered into this picture (IDE2p + M_ν + $N_{\rm eff}$) no significant changes are obtained, apart from the large anticorrelation between w_x and M_ν. The DE equation of state still prefers $w_x < -1$ with high significance. Finally, for both IDE2p and IDE2p + $M_\nu + N_{\rm eff}$ models we find that ξ_0 and ξ_a are consistent with zero, leading to a negligible preference for an interacting scenario.

The scenario IDE2q is quite different from the previous cases. Within this interaction scheme we find that none of the tensions (H_0, S_8) are alleviated. We do not find any evidence for an interaction among the dark sectors, since both the parameters ξ_0 and ξ_a, quantifying the interaction, are consistent with zero. An interesting outcome of this scenario is that it provides the most stringent bound on M_ν found in this study ($M_\nu < 0.116$ eV at 95% CL), which is obtained for the combination of CMB + R19.

Finally, to conclude, the bounds on the effective number of neutrino species $N_{\rm eff}$ as we see in almost all of the scenarios above are extremely robust and consistent with the standard value of $N_{\rm eff} = 3.046$ and are, therefore, completely unaffected by the dynamics of the dark sectors. However, the H_0 tension scenario, which for some cases in this work is alleviated, needs further investigation in light of other cosmological datasets. The excess of lensing in the CMB damping tail (see for instance [90]) might be an appealing investigation in this context.

ACKNOWLEDGMENTS

The authors thank the referee for some valuable comments aiming to improve the quality of the manuscript. W. Y. acknowledges the support from the National Natural Science Foundation of China under Grants No. 11705079 and No. 11647153. E. D. V. was supported by the European Research Council in the form of a Consolidator Grant with number 681431. O. M. is supported by the Spanish Grants No. FPA2017-85985-P and No. SEV-2014-0398 of the MINECO, by PROMETEO/2019/083 and by the European Union Horizon 2020 research and innovation program (Grant Agreements No. 690575 and No. 67489). S. P. was supported by the Science and Engineering Research Board (SERB), Government of India through the Mathematical Research Impact-Centric Support Scheme (MATRICS), File No. MTR/2018/000940.

[1] S. M. Carroll, Quintessence and the Rest of the World, Phys. Rev. Lett. **81**, 3067 (1998).
[2] C. Wetterich, The cosmon model for an asymptotically vanishing time dependent cosmological 'constant', Astron. Astrophys. **301**, 321 (1995).
[3] L. Amendola, Coupled quintessence, Phys. Rev. D **62**, 043511 (2000).
[4] L. Amendola and C. Quercellini, Tracking and coupled dark energy as seen by WMAP, Phys. Rev. D **68**, 023514 (2003).

[5] D. Pavón and W. Zimdahl, Holographic dark energy and cosmic coincidence, Phys. Lett. B **628**, 206 (2005).
[6] S. del Campo, R. Herrera, and D. Pavón, Toward a solution of the coincidence problem, Phys. Rev. D **78**, 021302 (2008).
[7] S. del Campo, R. Herrera, and D. Pavón, Interacting models may be key to solve the cosmic coincidence problem, J. Cosmol. Astropart. Phys. 01 (2009) 020.
[8] A. P. Billyard and A. A. Coley, Interactions in scalar field cosmology, Phys. Rev. D **61**, 083503 (2000).
[9] J. D. Barrow and T. Clifton, Cosmologies with energy exchange, Phys. Rev. D **73**, 103520 (2006).
[10] L. Amendola, G. C. Campos, and R. Rosenfeld, Consequences of dark matter-dark energy interaction on cosmological parameters derived from SNIa data, Phys. Rev. D **75**, 083506 (2007).
[11] J. H. He and B. Wang, Effects of the interaction between dark energy and dark matter on cosmological parameters, J. Cosmol. Astropart. Phys. 06 (2008) 010.
[12] J. Väliviita, E. Majerotto, and R. Maartens, Instability in interacting dark energy and dark matter fluids, J. Cosmol. Astropart. Phys. 07 (2008) 020.
[13] M. B. Gavela, D. Hernandez, L. Lopez Honorez, O. Mena, and S. Rigolin, Dark coupling, J. Cosmol. Astropart. Phys. 07 (2009) 034.
[14] E. Majerotto, J. Valiviita, and R. Maartens, Adiabatic initial conditions for perturbations in interacting dark energy models, Mon. Not. R. Astron. Soc. **402**, 2344 (2010).
[15] M. B. Gavela, L. L. Honorez, O. Mena, and S. Rigolin, Dark coupling and gauge invariance, J. Cosmol. Astropart. Phys. 11 (2010) 044.
[16] T. Clemson, K. Koyama, G. B. Zhao, R. Maartens, and J. Valiviita, Interacting dark energy: Constraints and degeneracies, Phys. Rev. D **85**, 043007 (2012).
[17] S. Pan, S. Bhattacharya, and S. Chakraborty, An analytic model for interacting dark energy and its observational constraints, Mon. Not. R. Astron. Soc. **452**, 3038 (2015).
[18] S. Pan and S. Chakraborty, Will there be again a transition from acceleration to deceleration in course of the dark energy evolution of the universe?, Eur. Phys. J. C **73**, 2575 (2013).
[19] W. Yang and L. Xu, Testing coupled dark energy with large scale structure observation, J. Cosmol. Astropart. Phys. 08 (2014) 034.
[20] W. Yang and L. Xu, Cosmological constraints on interacting dark energy with redshift-space distortion after Planck data, Phys. Rev. D **89**, 083517 (2014).
[21] R. C. Nunes and E. M. Barboza, Dark matter-dark energy interaction for a time-dependent EoS parameter, Gen. Relativ. Gravit. **46**, 1820 (2014).
[22] C. van de Bruck and J. Morrice, Disformal couplings and the dark sector of the universe, J. Cosmol. Astropart. Phys. 04 (2015) 036.
[23] R. C. Nunes, S. Pan, and E. N. Saridakis, New constraints on interacting dark energy from cosmic chronometers, Phys. Rev. D **94**, 023508 (2016).
[24] S. Kumar and R. C. Nunes, Probing the interaction between dark matter and dark energy in the presence of massive neutrinos, Phys. Rev. D **94**, 123511 (2016).
[25] S. Pan and G. S. Sharov, A model with interaction of dark components and recent observational data, Mon. Not. R. Astron. Soc. **472**, 4736 (2017).
[26] C. van de Bruck, J. Mifsud, and J. Morrice, Testing coupled dark energy models with their cosmological background evolution, Phys. Rev. D **95**, 043513 (2017).
[27] A. Mukherjee and N. Banerjee, In search of the dark matter dark energy interaction: a kinematic approach, Classical Quantum Gravity **34**, 035016 (2017).
[28] G. S. Sharov, S. Bhattacharya, S. Pan, R. C. Nunes, and S. Chakraborty, A new interacting two fluid model and its consequences, Mon. Not. R. Astron. Soc. **466**, 3497 (2017).
[29] S. Kumar and R. C. Nunes, Echo of interactions in the dark sector, Phys. Rev. D **96**, 103511 (2017).
[30] W. Yang, N. Banerjee, and S. Pan, Constraining a dark matter and dark energy interaction scenario with a dynamical equation of state, Phys. Rev. D **95**, 123527 (2017).
[31] W. Yang, S. Pan, and J. D. Barrow, Large-scale stability and astronomical constraints for coupled dark-energy models, Phys. Rev. D **97**, 043529 (2018).
[32] J. Mifsud and C. Van De Bruck, Probing the imprints of generalized interacting dark energy on the growth of perturbations, J. Cosmol. Astropart. Phys. 11 (2017) 001.
[33] C. Van De Bruck and J. Mifsud, Searching for dark matter-dark energy interactions: Going beyond the conformal case, Phys. Rev. D **97**, 023506 (2018).
[34] S. Kumar and R. C. Nunes, Observational constraints on dark matter–dark energy scattering cross section, Eur. Phys. J. C **77**, 734 (2017).
[35] W. Yang, S. Pan, and D. F. Mota, Novel approach toward the large-scale stable interacting dark-energy models and their astronomical bounds, Phys. Rev. D **96**, 123508 (2017).
[36] S. Pan, A. Mukherjee, and N. Banerjee, Astronomical bounds on a cosmological model allowing a general interaction in the dark sector, Mon. Not. R. Astron. Soc. **477**, 1189 (2018).
[37] W. Yang, S. Pan, and A. Paliathanasis, Cosmological constraints on an exponential interaction in the dark sector, Mon. Not. R. Astron. Soc. **482**, 1007 (2019).
[38] W. Yang, S. Pan, L. Xu, and D. F. Mota, Effects of anisotropic stress in interacting dark matter—dark energy scenarios, Mon. Not. R. Astron. Soc. **482**, 1858 (2019).
[39] W. Yang, S. Pan, R. Herrera, and S. Chakraborty, Large-scale (in) stability analysis of an exactly solved coupled dark-energy model, Phys. Rev. D **98**, 043517 (2018).
[40] W. Yang, N. Banerjee, A. Paliathanasis, and S. Pan, Reconstructing the dark matter and dark energy interaction scenarios from observations, Phys. Dark Universe **26**, 100383 (2019).
[41] M. Martinelli, N. B. Hogg, S. Peirone, M. Bruni, and D. Wands, Constraints on the interacting vacuumgeodesic CDM scenario, Mon. Not. R. Astron. Soc. **488**, 3423 (2019).
[42] A. Paliathanasis, S. Pan, and W. Yang, Dynamics of nonlinear interacting dark energy models, Int. J. Mod. Phys. D **28**, 1950161 (2019).
[43] S. Pan, W. Yang, C. Singha, and E. N. Saridakis, Observational constraints on sign-changeable interaction models and alleviation of the H_0 tension, Phys. Rev. D **100**, 083539 (2019).

[44] S. Kumar, R. C. Nunes, and S. K. Yadav, Dark sector interaction: A remedy of the tensions between CMB and LSS data, Eur. Phys. J. C **79**, 576 (2019).

[45] W. Yang, S. Pan, E. Di Valentino, B. Wang, and A. Wang, Forecasting interacting vacuum-energy models using gravitational waves, J. Cosmol. Astropart. Phys. 05 (2020) 050.

[46] W. Yang, S. Vagnozzi, E. Di Valentino, R. C. Nunes, S. Pan, and D. F. Mota, Listening to the sound of dark sector interactions with gravitational wave standard sirens, J. Cosmol. Astropart. Phys. 07 (2019) 037.

[47] J. D. Barrow and G. Kittou, Non-linear interactions in cosmologies with energy exchange, Eur. Phys. J. C **80**, 120 (2020).

[48] S. Pan, W. Yang, E. Di Valentino, E. N. Saridakis, and S. Chakraborty, Interacting scenarios with dynamical dark energy: Observational constraints and alleviation of the H_0 tension, Phys. Rev. D **100**, 103520 (2019).

[49] G. Papagiannopoulos, P. Tsiapi, S. Basilakos, and A. Paliathanasis, Dynamics and cosmological evolution in Λ-varying cosmology, Eur. Phys. J. C **80**, 55 (2020).

[50] W. Yang, E. Di Valentino, S. Pan, S. Basilakos, and A. Paliathanasis, Metastable dark energy models in light of Planck 2018: Alleviating the H_0 tension, arXiv:2001.04307.

[51] S. Pan, G. S. Sharov, and W. Yang, Field theoretic interpretations of interacting dark energy scenarios and recent observations, Phys. Rev. D **101**, 103533 (2020).

[52] S. Pan, J. de Haro, W. Yang, and J. Amorós, Understanding the phenomenology of interacting dark energy scenarios and their theoretical bounds, Phys. Rev. D **101**, 123506 (2020).

[53] S. Pan, W. Yang, and A. Paliathanasis, Nonlinear interacting cosmological models after Planck 2018 legacy release and the H_0 tension, Mon. Not. R. Astron. Soc. **493**, 3114 (2020).

[54] M. Lucca and D. C. Hooper, Tensions in the dark: Shedding light on dark matter-dark energy interactions, arXiv:2002.06127.

[55] W. Yang, O. Mena, S. Pan, and E. Di Valentino, Dark sectors with dynamical coupling, Phys. Rev. D **100**, 083509 (2019).

[56] E. Giusarma, M. Gerbino, O. Mena, S. Vagnozzi, S. Ho, and K. Freese, Improvement of cosmological neutrino mass bounds, Phys. Rev. D **94**, 083522 (2016).

[57] M. Gerbino, K. Freese, S. Vagnozzi, M. Lattanzi, O. Mena, E. Giusarma, and S. Ho, Impact of neutrino properties on the estimation of inflationary parameters from current and future observations, Phys. Rev. D **95**, 043512 (2017).

[58] S. Vagnozzi, E. Giusarma, O. Mena, K. Freese, M. Gerbino, S. Ho, and M. Lattanzi, Unveiling ν secrets with cosmological data: neutrino masses and mass hierarchy, Phys. Rev. D **96**, 123503 (2017).

[59] S. Vagnozzi, S. Dhawan, M. Gerbino, K. Freese, A. Goobar, and O. Mena, Constraints on the sum of the neutrino masses in dynamical dark energy models with $w(z) \geq -1$ are tighter than those obtained in ΛCDM, Phys. Rev. D **98**, 083501 (2018).

[60] E. Giusarma, S. Vagnozzi, S. Ho, S. Ferraro, K. Freese, R. Kamen-Rubio, and K. B. Luk, Scale-dependent galaxy bias, CMB lensing-galaxy cross-correlation, and neutrino masses, Phys. Rev. D **98**, 123526 (2018).

[61] S. Roy Choudhury and S. Choubey, Updated bounds on sum of neutrino masses in various cosmological scenarios, J. Cosmol. Astropart. Phys. 09 (2018) 017.

[62] S. Vagnozzi, T. Brinckmann, M. Archidiacono, K. Freese, M. Gerbino, J. Lesgourgues, and T. Sprenger, Bias due to neutrinos must not uncorrect'd go, J. Cosmol. Astropart. Phys. 09 (2018) 001.

[63] S. Vagnozzi, Cosmological searches for the neutrino mass scale, and mass ordering, arXiv:1907.08010.

[64] W. Yang, S. Pan, R. C. Nunes, and D. F. Mota, Dark calling Dark: Interaction in the dark sector in presence of neutrino properties after Planck CMB final release, J. Cosmol. Astropart. Phys. 04 (2020) 008.

[65] W. Yang, E. Di Valentino, O. Mena, S. Pan, and R. C. Nunes, All-inclusive interacting dark sector cosmologies, Phys. Rev. D **101**, 083509 (2020).

[66] S. Hagstotz, P. F. de Salas, S. Gariazzo, M. Gerbino, M. Lattanzi, S. Vagnozzi, K. Freese, and S. Pastor, Bounds on light sterile neutrino mass and mixing from cosmology and laboratory searches, arXiv:2003.02289.

[67] N. Aghanim *et al.* (Planck Collaboration), Planck 2018 results. VI. Cosmological parameters, arXiv:1807.06209.

[68] N. Aghanim *et al.* (Planck Collaboration), Planck 2018 results. VIII. Gravitational lensing, arXiv:1807.06210.

[69] N. Aghanim *et al.* (Planck Collaboration), Planck 2018 results. V. CMB power spectra and likelihoods, arXiv:1907.12875.

[70] F. Beutler, C. Blake, M. Colless, D. H. Jones, L. Staveley-Smith, L. Campbell, Q. Parker, W. Saunders, and F. Watson, The 6dF Galaxy survey: Baryon acoustic oscillations and the local Hubble constant, Mon. Not. R. Astron. Soc. **416**, 3017 (2011).

[71] A. J. Ross, L. Samushia, C. Howlett, W. J. Percival, A. Burden, and M. Manera, The clustering of the SDSS DR7 main Galaxy sample—I. A 4 per cent distance measure at $z = 0.15$, Mon. Not. R. Astron. Soc. **449**, 835 (2015).

[72] S. Alam *et al.* (BOSS Collaboration), The clustering of galaxies in the completed SDSS-III Baryon oscillation spectroscopic survey: Cosmological analysis of the DR12 galaxy sample, Mon. Not. R. Astron. Soc. **470**, 2617 (2017).

[73] A. G. Riess, S. Casertano, W. Yuan, L. M. Macri, and D. Scolnic, Large magellanic cloud cepheid standards provide a 1% foundation for the determination of the Hubble constant and stronger evidence for physics beyond ΛCDM, Astrophys. J. **876**, 85 (2019).

[74] A. Lewis and S. Bridle, Cosmological parameters from CMB and other data: A Monte Carlo approach, Phys. Rev. D **66**, 103511 (2002).

[75] A. Lewis, A. Challinor, and A. Lasenby, Efficient computation of CMB anisotropies in closed FRW models, Astrophys. J. **538**, 473 (2000).

[76] A. Gelman and D. Rubin, Inference from iterative simulation using multiple sequences, Stat. Sci. **7**, 457 (1992).

[77] E. Di Valentino, A. Melchiorri, O. Mena, and S. Vagnozzi, Nonminimal dark sector physics and cosmological tensions, Phys. Rev. D **101**, 063502 (2020).

[78] T. M. C. Abbott *et al.* (DES Collaboration), Dark energy survey year 1 results: Cosmological constraints from Galaxy clustering and weak lensing, Phys. Rev. D **98**, 043526 (2018).

[79] M. A. Troxel *et al.* (DES Collaboration), Dark energy survey year 1 results: Cosmological constraints from cosmic shear, Phys. Rev. D **98**, 043528 (2018).

[80] H. Hildebrandt *et al.*, KiDS-450: Cosmological parameter constraints from tomographic weak gravitational lensing, Mon. Not. R. Astron. Soc. **465**, 1454 (2017).

[81] K. Kuijken *et al.*, Gravitational lensing analysis of the kilo degree survey, Mon. Not. R. Astron. Soc. **454**, 3500 (2015).

[82] I. Fenech Conti, R. Herbonnet, H. Hoekstra, J. Merten, L. Miller, and M. Viola, Calibration of weak-lensing shear in the kilo-degree survey, Mon. Not. R. Astron. Soc. **467**, 1627 (2017).

[83] C. Heymans *et al.*, CFHTLenS: The Canada-France-Hawaii telescope lensing survey, Mon. Not. R. Astron. Soc. **427**, 146 (2012).

[84] T. Erben *et al.*, CFHTLenS: The Canada-France-Hawaii telescope lensing survey–Imaging data and catalogue products, Mon. Not. R. Astron. Soc. **433**, 2545 (2013).

[85] S. Joudaki *et al.*, CFHTLenS revisited: Assessing concordance with Planck including astrophysical systematics, Mon. Not. R. Astron. Soc. **465**, 2033 (2017).

[86] M. Asgari *et al.*, KiDS+VIKING-450 and DES-Y1 combined: Mitigating baryon feedback uncertainty with COSEBIs, Astron. Astrophys. **634**, A127 (2020).

[87] G. Mangano, G. Miele, S. Pastor, T. Pinto, O. Pisanti, and P. D. Serpico, Relic neutrino decoupling including flavor oscillations, Nucl. Phys. **B729**, 221 (2005).

[88] P. F. de Salas and S. Pastor, Relic neutrino decoupling with flavour oscillations revisited, J. Cosmol. Astropart. Phys. 07 (2016) 051.

[89] E. Di Valentino, A. Melchiorri, O. Mena, and S. Vagnozzi, Interacting dark energy in the early 2020s: A promising solution to the H_0 and cosmic shear tensions, Phys. Dark Univ. **30**, 100666 (2020).

[90] P. Motloch and W. Hu, Tensions between direct measurements of the lens power spectrum from Planck data, Phys. Rev. D **97**, 103536 (2018).